Journal of Engineering Science and Technology
Vol. 12, No. 3 (2017) 780 - 796
© School of Engineering, Taylor's University

FABRICATION OF CNTS BY TOLUENE DECOMPOSITION IN A NEW REACTOR BASED ON AN ATMOSPHERIC PRESSURE PLASMA JET COUPLED TO A CVD SYSTEM

FELIPE RAMÍREZ-HERNÁNDEZ[1,*], FRANKLIN MUÑOZ-MUÑOZ[1], GERARDO SOTO[1]

[1]Centro de Nanociencias y Nanotecnología UNAM, Km 107 Carretera Tijuana-Ensenada s/n, Ensenada, B.C., C.P. 22800, México
*Corresponding Author: framirez@cnyn.unam.mx

Abstract

Here, we present a method to produce carbon nanotubes (CNTs) based on the coupling between two conventional techniques used for the preparation of nanostructures: an arc-jet as a source of plasma and a chemical vapour deposition (CVD) system. We call this system as an "*atmospheric pressure plasma (APP)-enhanced CVD*" (APPE-CVD). This reactor was used to grow CNTs on non-flat aluminosilicate substrates by the decomposition of toluene (carbon source) in the presence of ferrocene (as a catalyst). Both, CNTs and by-products of carbon were collected at three different temperatures (780, 820 and 860 °C) in different regions of the APPE-CVD system. These samples were analysed by thermogravimetric analysis (TGA and DTG), scanning electron microscopy (SEM) and Raman spectroscopy in order to determine the effect of APP on the thermal stability of the as-grown CNTs. It was found that the amount of metal catalyst in the synthesised CNTs is reduced by applying APP, being 820 °C the optimal temperature to produce CNTs with a high yield and carbon purity (95 wt. %). In contrast, when the synthesis temperature was fixed at 780 °C or 860 °C, amorphous carbon or CNTs with different structural defects, respectively, was formed through APEE-CVD reactor. We recommended the use of non-flat aluminosilicate particles as supports to increase CNT yield and facilitate the removal of deposits from the substrate surface. The approach that we implemented (to synthesise CNTs by using the APPE-CVD reactor) may be useful to produce these nanostructures on a gram-scale for use in basic studies. The approach may also be scaled up for mass production.

Keywords: Carbon nanotubes; CVD; Atmospheric pressure plasma; Commercial arc-jet.

Nomenclatures

CVD (zone)	Zone of CVD furnace
CVD-S820	Sample synthesised at 820 deg. Celsius extracted from spheres of CVD furnace
CVD-S860	Sample synthesised at 860 deg. Celsius extracted from spheres of CVD furnace
CVD-T780	Sample synthesised at 780 deg. Celsius extracted from inner walls of CVD furnace
$CVD\text{-}T820_{with\ plasma}$	Sample synthesised at 820 deg. Celsius extracted from inner walls of CVD furnace and plasma on
$CVD\text{-}T820_{without\ plasma}$	Sample synthesised at 820 deg. Celsius extracted from inner walls of CVD furnace and plasma off
CVD-T860	Sample synthesised at 860 deg. Celsius extracted from inner walls of CVD furnace
$CVD\text{-}T860_{with\ plasma}$	Sample synthesised at 860 deg. Celsius extracted from inner walls of CVD furnace and plasma on
$CVD\text{-}T860_{without\ plasma}$	Sample synthesised at 860 deg. Celsius extracted from inner walls of CVD furnace and plasma off
M_{res}	Residual mass, kg
P (zone)	Zone of incidence of the atmospheric plasma
PCVD (zone)	Zone between atmospheric plasma incidence and CVD furnace
PCVD-T860	Sample synthesised at 860 deg. Celsius extracted from inner walls of zone between P and CVD
P-T780	Sample synthesised at 860 deg. Celsius extracted from spheres of plasma incidence zone
P-T860	Sample synthesised at 860 deg. Celsius extracted from inner walls of plasma incidence zone
T_{max}	Temperature of maximum rate of oxidation, ^{o}C
T_o	Temperature of oxidation, ^{o}C
T_{onset}	Weight loss onset temperature, ^{o}C

Abbreviations

APP	Atmospheric Pressure Plasma
APPE	Atmospheric Pressure Plasma Enhanced
CNTs	Carbon nanotubes
CO	Carbon monoxide
CVD	Chemical Vapour Deposition
DC	Direct Current
DTG	Differential Thermogravimetric Analysis
EDX	X-ray Energy dispersive Analysis
SEM	Scanning Electron Microscope
slm	Standard Litres Per Minute
TGA	Thermogravimetric Analysis

1. Introduction

Carbon nanotubes (CNTs) are of great interest due to their unique electrical, mechanical, thermal and chemical properties. Based on experimental and

theoretical investigations, CNTs are considered to be the key to the development of novel technological applications. Such applications include super-strong fibres, catalysts, molecular switches, functional components for nanoscale electronic devices, additives for high-strength polymer composites, etc. [1, 2]. Both basic research and the exploration of potential applications have accelerated the production of high-quality CNTs. However, there still is a need to fabricate these nanostructures on a large scale. To date, relatively large amounts of CNTs can be prepared using any one of three main methods: laser ablation [3], arc-discharge [4, 5] and chemical vapour deposition (CVD) [7]. Among these, CVD methods enable control of the growth of nanotubes by adjusting the parameters involved in the CVD process. Recent studies have reported the growth of single-walled CNTs by CVD as a breakthrough in terms of the production of regular nanostructures with high purity [6, 7].

The CVD method is able to grow CNTs at a low cost compared with other methods that require vacuum systems and complex equipment. Nevertheless, an atmospheric pressure plasma enhanced CVD (APPE-CVD) system can be implemented to further reduce the amount of energy required to grow CNTs. Consequently, these can enable the production of nanostructures at industrial scales. Carbon nanotubes were grew using a newly developed APPE-CVD system by Shin and co-workers [8]. The system used a helium (He) plasma, acetylene as a carbon feedstock, and p-type Si/SiO2 wafers coated with iron (Fe) (by sputtering) as supports. In this research, it was found that APP facilitated the dissociation of the carbon source gas, resulting in CNTs with growth rates and yields that were higher than those of CNTs grown by thermal or low plasma power CVD. Due to the ability of non-equilibrium plasmas to produce active species at relatively low temperatures, an APP source used as an arc-jet avoids the requirement of complex equipment to reach vacuum conditions [9]. This method has been applied to produce highly crystallised CNTs using methane [10] ethylene [11] or CO [12] as a carbon source. The use of plasma for oxidative functionalisation of multi-walled CNTs has also been reported [13].

The use of non-flat micro-sized materials as supports is considered to be a promising approach for large scale production of CNTs. This is due to the large surface/volume ratio exposed on the support surface [14]. The advantages of CNT synthesis on such supports include the production of large amounts nanotubes, improvement of the properties of the composite material, and regeneration or reuse of the support-catalyst system.

The APP effects on CNT synthesis using our newly developed APPE-CVD reactor were investigated. The APPE-CVD reactor developed for CNT synthesis comprises a DC plasma torch coupled to thermal CVD equipment to perform the atomisation, formation of radical species and subsequent precipitation of carbon from aerosol mixtures. Inexpensive equipment to implement the APPE-CVD reactor was used, in order to lower production costs and to grow CNTs for commercial use.

2. Materials and Methods

2.1. Description of the APP-CVD reactor for carbon nanotube growth

Carbon nanotubes were synthesised in a reactor that contained a commercial DC plasma torch (Multiplaz® 3500, Switzerland) coupled at the end of a hot-wall

horizontal CVD chamber. The chamber was a quartz tube (22 mm internal diameter and 450 mm effective heating zone length) heated by an electric furnace. A pneumatic jet nebuliser was placed normal at the plasma plume and was used to generate a rich carbon mixture mist through the tube. A water trap system was connected to the free end of the reaction tube to collect elutriated fine particles and to warn of the presence of residual gases and possible gas leakage during each run. Figure 1 shows a schematic of the experimental arrangement of our APPE-CVD reactor.

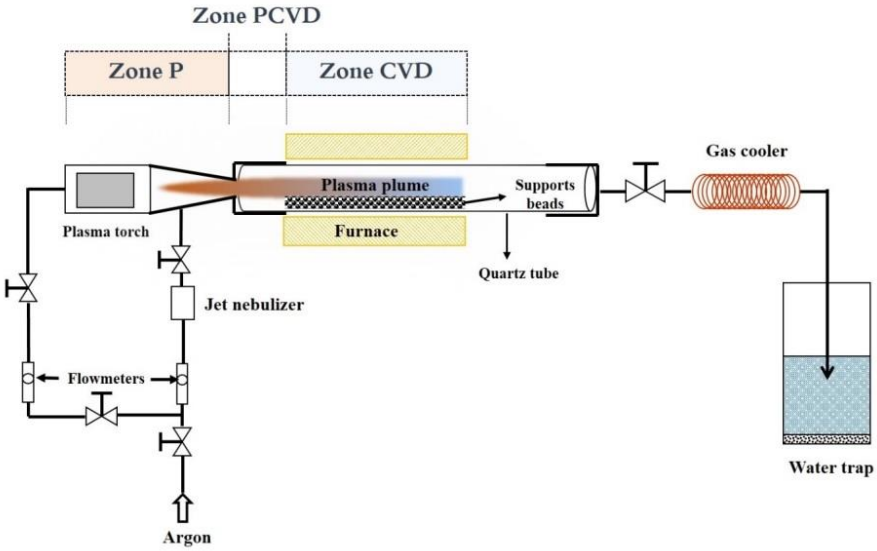

Fig. 1. Schematic of the experimental arrangement of the horizontally aligned APPE-CVD reactor for CNT synthesis. Three zones are distinguished: plasma (Zone P), CVD chamber (Zone CVD) and the boundary region labelled as PCVD.

2.2. Chemicals and general carbon nanotube synthesis procedure

A batch of 10 g of aluminosilicate ceramic beads (King's Ceramics & Chemicals, China), containing Al_2O_3:SiO_2 (93:7 wt. %) with traces of MgO, mean diameter of 0.7 mm (0.3 to 0.8) and specific weight 3.62 g/cm^3, was fed into the tube. The CVD chamber was preheated to the desired temperature (780, 820 or 860 °C) and purged with an argon (Praxair 99.99 %) flow of 0.25 standard litres per minute (slm) for 5 min. Once the chamber temperature was set, the argon flow was set at 1.0 slm through the plasma torch, and a pre-established power of 100 W was supplied to the DC source to ignite the plasma. The pneumatic nebuliser was fed with 12 mL of a solution containing 2.5 wt. % of ferrocene (Aldrich 98 %) as a catalyst precursor, in toluene (Aldrich 99.8 %) as a carbon feedstock. An argon flow (3 slm for 20 min) was used to generate a mist through the nebuliser and to carry the aerosol into the tube. Carbonaceous black film grew from the support surface and/or inner wall of the quartz tube. This was mechanically removed by scraping with a steel spatula.

2.3. Experimental series

An effect of energy gradient induced by the APP was distinguished in three zones of formation of CNT, presented in Fig. 1. The first one is the plasma region (zone P) in which energy is supplied to the carbon source precursor for its molecular dissociation. The second region is the CVD chamber (zone CVD). A third zone is identified as "zone PCVD" that corresponds to the quartz tube section between the furnace (zone "CVD") and the plasma torch (zone "P"). Two sets of experiments were carried out to determine the influence of 1) furnace temperature and 2) APP on the characteristics of the synthesised CNTs. In the first set of experiments, materials grew only in the "CVD" zone. The collected materials were labelled as "*X-Sy*" or "*X-Ty*", with "*X*" being the reactor zone ("CVD"), "*S*" indicating carbonaceous materials collected from the aluminosilicate bead support, "*T*" referring to black films obtained from the inner walls of the quartz tube and "*y*" being the furnace temperature (820 or 860 Celsius). No carbonaceous material was found at 780 °C to provide *CVD-S780*. Table 1 shows the assignments of the samples in the first set of experiments.

Table 1. Sample assignation of the first set of experiments (synthesis of CNT with CVD only).

	Materials extracted at CVD zone from	
Furnace temperature °C	**beads**	**reactor walls**
780	-	CVD-T780
820	CVD-S820	CVD-T820
860	CVD-S860	CVD-T860$_a$

a For the second set of experiments, CVD-T860 $_{without\ plasma}$ can be used instead to refer to CVD-T860.

In the second set of experiments, carbonaceous materials grew in multiple zones ("P" and/or "CVD" and/or "PCVD") and the materials were collected only from the inner walls of the quartz tube, and the sample labelling was the same as in the first set of experiments: "*X-Ty*", with "*X*" indicating the reactor zone ("P", "CVD" or "PCVD"), "*T*" for the black films obtained from the inner walls of the quartz tube and "*y*" the furnace temperature (780, 820 or 860 C). No carbonaceous material was found in the PCVD zone at 780 and 820 °C to render *PCVD-T780* and *PCVD-T820*. Table 2 shows the names of the samples for the second set of experiments.

Table 2. Sample assignation of the second set of experiments (synthesis of CNT with APP and CVD).

	Materials extracted at reactor walls from zone		
Furnace temperature °C	**P**	**CVD**	**PCVD**
780	P-T780	CVD-T780	PCVD-T780
820	P-T820	CVD-T820	-
860	P-T860	CVD-T860$_b$	PCVD-T860$_b$

B For the second set of experiments, CVD-T860 $_{without\ plasma}$ and PCVD-T860 $_{without\ plasma}$ can be used instead to refer to CVD-T860 and PCVD-T860, respectively.

2.4. Microstructural analysis

A scanning electron microscope (SEM, JEOL, JSM-5300) equipped with an Energy-dispersive X-ray (EDX) analyser (ThermoNoran SuperDry II; resolution 139 eV) was used to examine the sample morphology and for qualitative/semiquantitative analysis of the elemental chemical composition. A transmission electron microscope (TEM, JEOL-JEM 2100F) was employed for high resolution examination of the nanostructure of the CNTs. Defects, diameters, lengths and wall numbers were examined. Determination of D, G, an RMB bands were obtained from Raman spectra of as-synthesised CNTs bundles. The spectra were collected using a laser Micro-Raman spectrometer (Horiba, Olympus BX41, excitation wavelength = 638 nm).

2.5. Thermal analysis of CNTs

A thermogravimetric analyser (TA Instruments Q600) was used to determine thermal decomposition of the CNTs (~ 4 mg sample size). Thermogravimetric analysis of samples were performed under air (as atmosphere) over a temperature range of 100 °C to 800 °C, using a heating ramp of 4°C min^{-1}. The residual mass (M_{res}) and the weight loss onset temperature (T_{onset}) were quantified from thermogravimetric analysis (TGA) measurements, and the temperature of the maximum rate of oxidation (T_{max1}) was identified as the maximum point of the differential analysis (DTG) plot. The oxidation temperatures (T_o) of the CNT samples were estimated from the averages of their respective T_{onset} and T_{max} values.

3. Results and Discussion

3.1. Effect of furnace temperature on CNT formation (experimental set 1)

A carbonaceous material (with the appearance of a uniform black film) grew randomly from the surface of the aluminosilicate support and/or the inner surface of the quartz tube, depending on the furnace temperature setting.

When the furnace temperature was fixed at 780 °C, a small amount of black film was formed on the surrounding reaction tube (*CVD-T780*) but not on the support surface. This indicates that the carbon and iron (Fe) atoms that are released by the pyrolysis of toluene and ferrocene gas, respectively, do not accumulate on the aluminosilicate beads at this temperature. At a temperature of 820 °C, the carbonaceous material grew simultaneously on the support surfaces and on the surrounding reaction tube, to produce *CVD-S820* and *CVD-T820*, respectively. For *CVD-S820*, Fig. 2(a), the material grew with high yields, forming islands on each aluminosilicate bead. This indicates that the catalyst deposition proceeded via island nucleation and coalescence [15]. Figure 2(b) shows a picture of the carbonaceous powders collected from the inner walls of the quartz tube.

Figure 3(a) shows a low magnification image of a pristine aluminosilicate bead as a reference. A high magnification image is shown in Fig. 3(b). After the growth process at 820 °C, an outer coating that forms islands surrounding the aluminosilicate bead is clearly visible, Fig. 3(c). The black film thickness, for *CVD-S820*, was measured to be approximately 0.2 mm. Figure 3(d) shows that

the spongy and rough cover of carbonaceous film consists of bunches of cylindrical graphite shells (CNTs). Figure 3(e) shows an SEM image of the carbonaceous film that grew on the aluminosilicate support at a temperature of 860 °C to render *CVD-S860*. Figure 3(f) shows a high magnification SEM image of the film coating. The film exhibits low density, nanotubes with various diameters, and catalyst coarsening.

(a) CVD-820S.

(b) CVD-820T.

(c) CVD-860S.

(d) CVD-860T.

Fig. 2. Pictures showing the carbonaceous deposits formed on (a) and (c) aluminosilicate bead supports, or (b) and (d) from the inner walls of the quartz tube in the CVD zone of the APPE-CVD reactor (Codes as in Table 1).

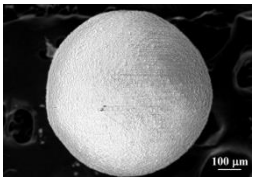

(a) Aluminosilicate bead.

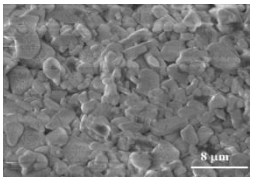

(b) Aluminosilicate bead (surface).

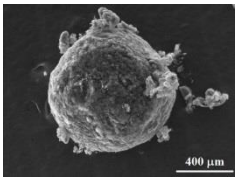

(c) CVD-820S.

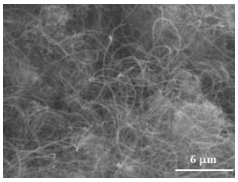

(d) CVD-820S (surface).

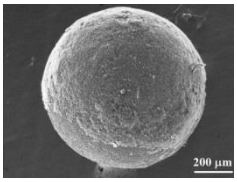

(e) CVD-860S.

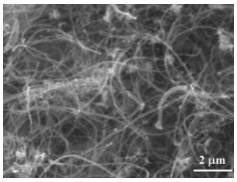

(f) CVD-860S (surface).

Fig. 3. SEM images of an aluminosilicate bead (a) and (b) before and (c) to (f) after coating with carbonaceous deposits in the APPE-CVD reactor. (Codes as in Table 1).

The EDX spectrum in Fig. 4 shows the presence of elemental C (0.268 keV) that arises mainly from the carbon source; O (0.533 keV) and Al (1.488 keV) which come from the substrate; and Fe (6.401 keV) from the catalyst precursor. The chemical compositions of *CVD-S820* and *CVD-S860* (as measured by EDX analysis) was summarised in Table 3. The higher amount of Fe in *CVD-S860* indicates that, at 860 °C, the catalyst atoms interact more strongly with themselves than they do with the carbon atoms from the vapour to form a metal-carbon solid solution. This agrees with the observations from the SEM images, Figs. 3(c) to (f). EDX analysis also revealed that other impurities are not present in the synthesis process.

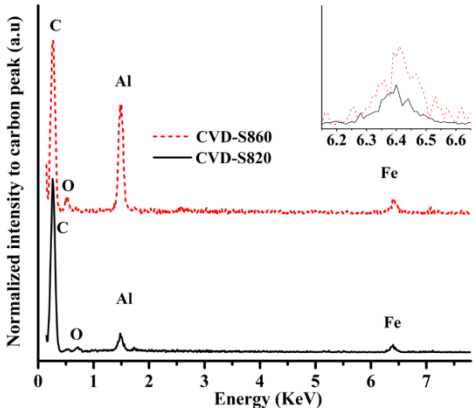

Fig. 4. EDX signal profiles for Al, O, C, and Fe elements found on an aluminosilicate support coated with carbonaceous material formed at 820 or 860 °C using the APPE-CVD reactor.

Table 3. Results (atomic % and weight %) of the EDX analysis of aluminosilicate supports coated with carbonaceous deposit formed in the CVD chamber of the APPE-CVD reactor at an operating temperature of 820 (CVD-S820) or 860 °C (CVD-S860).

	C		O		Al		Fe	
Sample	**Atom %**	**Wt. %**	**Atom %**	**Wt. %**	**Atom %**	**Wt. %**	**Atom %**	**Wt. %**
CVD-S820	94	85.9	2.8	3.5	1.2	2.3	2	8.3
CVD-S860	87	75.5	6	7	5	9.7	2	7.8

Thermal degradation curves for samples *CVD-T780*, *CVD-T820* and *CVD-T860* was compared in Fig. 5. The results of the thermal stability analysis for all of the samples that were analysed was summarised in table 4. Residual mass (M_{res}) is determined mainly by the presence of Fe particles in the sample. As a result of, *CVD-T780*, *CVD-T820* and *CVD-T860* have oxidation temperatures (T_{onset}) of ~ 341, 576 and 533 °C, respectively, Fig. 5(a) and Table 2. M_{res} was found to be approximately 31.0 wt. % for *CVD-T780*, indicating that the conversion of toluene into solid carbon is not very high at 780 °C. An M_{res} of ~ 6.0 wt. % was found for both *CVD-T820* and *CVD-T860*. However, *CVD-T820*

presented a stepwise weight loss at 619 °C in the DTG plot, Fig. 5(b). This was assigned to CNT formation [16]. For *CVD-S860*, two peaks were observed, one at 561 °C (70 % weight loss) and other at 621 ° C (18 % weight loss). These indicate that the carbonaceous film coating is composed of two different types of CNTs. The DTG peaks observed in the range between 300 and 450 °C, Fig. 5(b) correspond to the oxidation of amorphous carbon [17, 18]. It is know that CNTs tend to oxidise at higher temperatures than amorphous carbon. This is because CNTs have smaller numbers of active sites for oxidation [19].

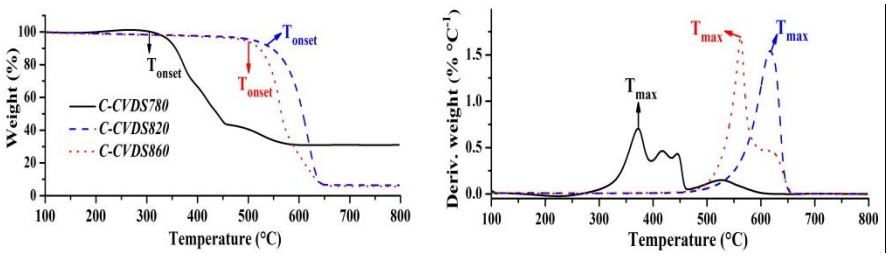

(a) TGA plot. **(b) DTG Plot.**

Fig. 5. (a) TGA and (b) DTG degradation curves of carbonaceous material extracted from the inner walls of quartz tube (CVD-T780) or the alumino-silicate surface (CVD-S820 and CVD-S860). These were synthesised at a specific operating temperature of the APPE-CVD reactor: 780, 820 or 860 °C. Codes as in Table 4.

Next, results were compared with the literature, starting from the lowest reaction temperature (of 780°C): The amount of carbonaceous material in the sample CVD-T780 (obtained in our APPE-CVD reactor) is consistent with a slow diffusion of carbon and Fe atoms into the CVD chamber. It was reported the synthesis of aligned MWCNTs containing a low concentration of single wall CNTs (SWCNTs) by Singh et al. [20]. They found that growth occurs primarily via a base-growth mechanism in which the initial deposition of ferrocene is thought to provide nucleation sites for the growth of nanotubes. Other previous studies of the CVD synthesis of carbon fibres and nanotubes was proposed that the mechanism of growth involves absorption, decomposition of hydrocarbon gas on a catalyst particle, and diffusion of carbon atoms into the catalyst bulk from a supersaturated catalyst surface [7]. It was thought that these steps apply to our current process.

When the synthesis temperature was fixed at 820 °C, the clusters of Fe particles served as a catalyst surface for nanotube growth. The high temperature enabled the supersaturation of carbon and catalyst atoms, by increasing the speed with which they spread across the CVD chamber. This led to CNT growth over the entire system (inner walls of the tube plus the aluminosilicate beads). It was observed that heating above a certain temperature causes clusters to coalesce and form macroscopic islands [21]. This process is controlled by cluster diffusion and depends on parameters such as their density and diffusion coefficient at a given substrate temperature. The diffusion terminates when the island shape reaches a minimum energy configuration for the specific annealing conditions [22]. The

growth temperature of 820 °C results in the highest number of CNTs per unit area with similar outer diameters. In contrast, the inhomogeneous set of CNTs that were obtained at 860 °C was attributed to un-catalysed thermal decomposition of the carbon source (toluene). This effect causes pyrolytic over coating of the underlying structures (including other nanotubes). It was reported similar results for CNT synthesis by a chemical injection CVD method, at a furnace temperature of 850 °C by Singh et al. [23].

Finally, a brief discussion of yield was carried out: In our current work (which is directed at high-yield CNT synthesis by coupling two different techniques without focusing on choosing the best material as support), CNT mass yields of between 0.3 and 0.5 g were achieved. This was done by feeding the APPE-CVD reactor with 10 g of non-porous aluminosilicate (Al_2O_3:SiO_2) beads. In comparison, it was described CNT production of 0.26 g using 40 g of Al_2O_3 beads with 0.5-mm diameters at a reaction temperature of 820 °C by Kim et al. [14]. These yields are lower than the values obtained in our work for the same type of flat substrate. Moreover, it was reported higher yields for CNT growth by aerosol-assisted CVD at low temperature, using micro-spherical alumina (Al_2O_3) particles or micro-platelet silicon carbide (SiC) particles (with 2-5 μm diameters) as supports by Dichiara and Bai [24]. They reported the production of 0.42 g with 0.4 g of beads, argued that the volume/area ratio increased the yield due to an increase in reactivity at the catalytic surface.

3.2. Effect of APP on CNTs formation (experimental set 2)

In order to determine the effect of the APP on the characteristics of the synthesised CNTs, the solid deposits that were formed in the "P", "CVD" or "PCVD" zones (after reaction at 780, 820 or 860 °C and with the plasma on), were collected and subsequent analysed by TGA, DTG and Raman spectroscopy. Quantitative weight loss data (M_{res}, T_{onset}, T_o *and* T_{max}) for the samples are presented in Table 4.

Table 4. Results of TGA and DTG analysis of carbonaceous materials synthesised by APPE-CVD reactor.

Code	T_{onset} (°C)	T_{max1} (°C)	T_o (°C)	T_{max2} (°C)	T_{max3} (°C)	T_{max4} (°C)	M_{res}
P-T780	271	369	320	-	-	-	19
CVD-T780	308	374	341	415	448	531	43
CVD-S820	532	619	576	-	-	-	6
CVD-T820$_{with\ plasma}$	533	620	577	-	-	-	6.1
CVD-T820$_{without\ plasma}$	533	600	567	-	-	-	28
P-T860	312	381	347	-	-	-	4.7
PCVD-T860	330	378	354	563	-	-	13.2
CVD-S860	504	561	533	621	-	-	6
CVD-T860	505	563	534	623	-	-	5.1
CVD-T860$_{without\ plasma}$	465	576	521	609	-	-	5

The weight loss, differential weight loss and Raman spectra profiles for the samples *P*-T780 and *CVD-T780* are shown in Figs. 6(a)-(c), respectively. At this temperature, there was no carbonaceous deposit formed in the PCVD region. For *CVD-T780* sample, the M_{res} estimated from the TGA plot was 19 %, and a weight loss region was observed in the DTG profile at 369 °C (T_{max}). Three peaks (T_{max1}, T_{max2}, T_{max3}) were observed for weight loss of *CVD-T780* between 300 and 465 °C. The weight losses were 43 % of the total mass and correspond to amorphous carbon. A peak between 465 and 580 °C (M_{res} = 31 %) corresponds to a small fraction of crystalline carbon (being CNTs). Two bands in the Raman spectrum for *CVD-T780* are shown in Fig. 6(c): a disordered band (D-band) at 1334 cm^{-1} and a graphitised band (G-band) at 1598 cm^{-1}. These can be attributed to amorphous carbon (or sp^2 carbon structures in the presence of any defects) and a form of crystalline carbon (CNTs), respectively [25]. A comparison between *CVD-T820* in the presence and in the absence of plasma to render $CVD\text{-}T820_{with\ plasma}$ and $CVD\text{-}T820_{without\ plasma}$ was shown in Fig. 7. Two types of carbonaceous materials tend to oxidise at similar temperatures, Fig. 7(a) and (b), both with a weight loss region between 600 and 617 °C in the DTG profile (Table 4).

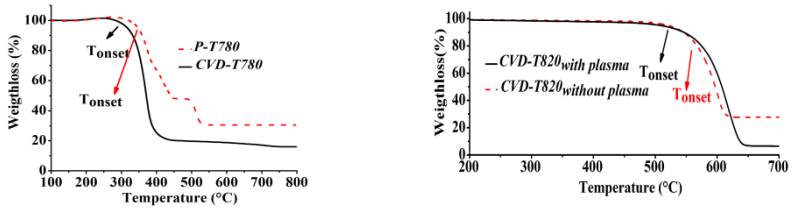

(a) TGA plot.

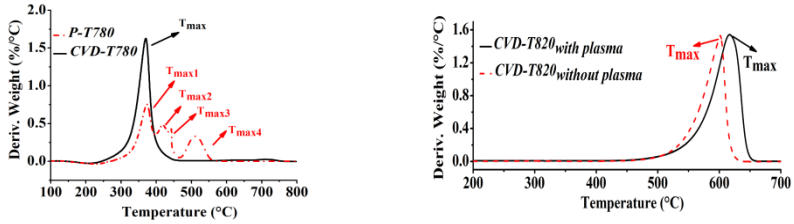

(b) DTG plot.

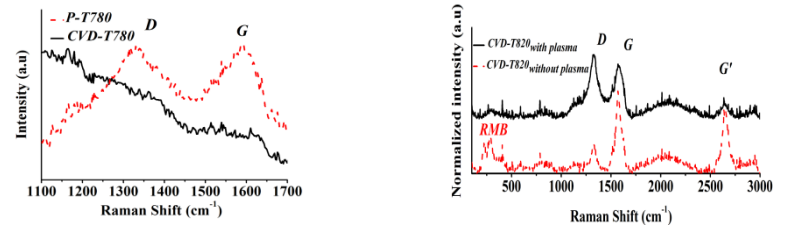

(c) Raman spectrum.

Fig. 6. (a) TGA, (b) DTG and (c) Raman spectrum profiles for carbonaceous materials synthesised in the zone P (P-T780) and in the CVD chamber (CVD-T780). (Codes as in Table 2)

Fig. 7. (a) TGA, (b) DTG and (c) Raman spectrum profiles for carbonaceous materials synthesised in the CVD chamber (CVD-T820) in the presence or absence of plasma. (Codes as in Table 2)

For CVD-$T820_{without\ plasma}$, 28.0 wt. % (M_{res}) of the sample is composed of iron catalyst particles, while for $CVD\text{-}T820_{\ with\ plasma}$, only 6.1 wt. % of the whole sample is the catalyst. Raman spectra in which several bands are observed are shown in Fig. 7(c): RBM peaks between 200 and 420 cm^{-1}, D-band at 1328 cm^{-1}, G-band at 1571 cm^{-1} and G´-band at 2640 cm^{-1}.

Based on the TGA/DTG results, Fig 6(a) and (b), the nucleation of CNTs did not occur with just the APP enthalpy by itself. Instead, APP coupled with CVD at 780 °C produced three types of amorphous carbon which oxidise between 300 and 465 °C. Adding the radiant power of APP to the CVD chamber results in the formation of more CNTs, Fig 6(a), than in the case of CVD alone, Fig 5(a). This increased CNT formation from 10.9 to 18.8 %. Raman analysis, Fig. 6(c) was indicated that a fraction of amorphous carbon and CNTs co-exist in the unpurified product (that results from the combined effect of APP and CVD).

A TEM image of the sample $CVD\text{-}T820_{with\ plasma}$ that exemplified the low iron content of the resulting CNTs is shown in Fig. 8(a). The CNTs are 5-10 nm in diameter and a few μm in length. In contrast, a TEM image of the sample $CVD\text{-}T820_{without\ plasma}$, Fig. 8(b), shows agglomeration of iron catalysts (product of the dissociation process in the APP) in the resulting CNTs. Based on the TGA results of Figs. 7(a) and (b) and the TEM images of Figs. 8(a) and (b), the CNTs synthesised by APP-enhanced CVD contain less metal catalyst compared with CNTs produced by using CVD alone. The use of a plasma causes the radicalisation of hydrocarbon species before they reach the CVD chamber. This causes higher graphitisation and prevents the agglomeration of the fragmented hydrocarbons, resulting in reduced accumulation of catalyst particles in the sample.

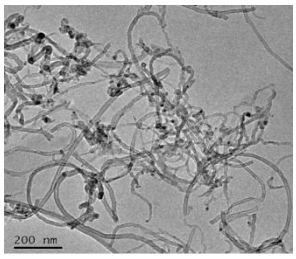

(a) CVD-T820 $_{with\ plasma}$.

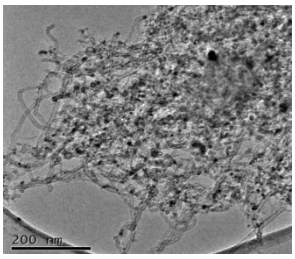

(b) CVD-T820 $_{without\ plasma}$.

Fig. 8. TEM images of CNTs in the samples: (a) CVD-T820 $_{with\ plasma}$ and (b) CVD-T820 $_{without\ plasma}$. These show the difference in iron content between CNTs produced in both states (plasma on/off) at 820°C.

Accordingly, the small shift of T_{max} in the DTG plot in Fig. 7(b) (from 620 °C for $CVD\text{-}T820_{with\ plasma}$ to 600 °C for $CVD\text{-}T820_{without\ plasma}$) may be caused by the catalytic effect of the metal during the thermal oxidisation of carbon. An increase in the amount of metal in the sample reduces its oxidation temperature [26]. The Raman spectra in Fig. 7(c), for the samples $CVD\text{-}T820_{with\ plasma}$ and $CVD\text{-}T820_{without\ plasma}$, reveals that the D-band may be attributed to defects in the nanotubes or in the curved graphite sheets, to amorphous carbon film covering the template surface, or to random orientation of the nanotubes [27]. The G-band indicated the formation of graphitised structures. The G´-peak at 2640 cm^{-1} (i.e., approx. 2x1328 cm^{-1}) is attributed to second order scattering of the G-line, while

the band observed at 2931 cm^{-1} can be caused by a combination of the D-line and the G-line (i.e., approx. 1328 cm^{-1} + 1571 cm^{-1}) [28]. The peaks between 211 and 419 cm^{-1} can be assigned to RBM bands that correspond to single wall CNTs (SWCNTs) or the innermost tube of multiwall CNTs (MWCNTs) [29]. However, TGA/DTG results did not show that SWCNTs and MWCNTs co-exist in the unpurified products, Figs. 7(a) and (b). The intensities of RBM, G- and G´-bands were drastically reduced when the CNTs were synthesised in the presence of plasma (*CVD-T820*$_{with\ plasma}$), indicating that the combined effect of APP and CVD produces CNTs with defects that lower the crystal symmetry of the lattice [30].

A TEM image of few walled CNTs (FWCNTs) observed in the sample *CVD-T820*$_{without\ plasma}$ are shown in Fig. (9). The observed FWCNTs are 3-6 nm in diameter and contain 2 to 5 walls on average.

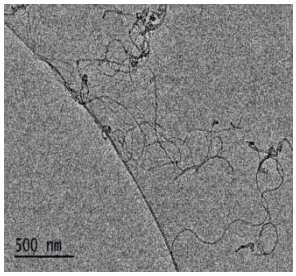

(a) isolated few walled CNTs (FWCNTs).

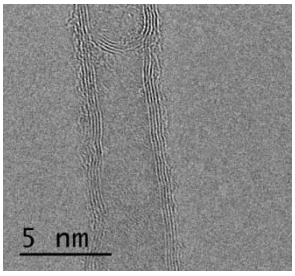

(b) Four walled CNT with amorphous carbon in the walls.

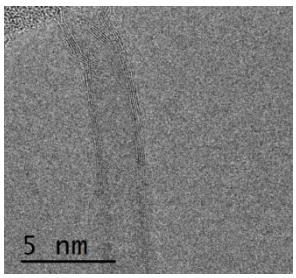

(c) Four walled CNT with defects.

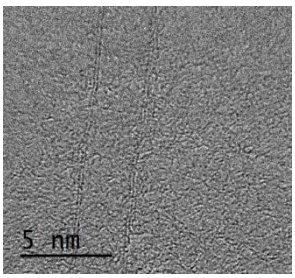

(d) Two walled CNT.

Fig. 9. TEM and HR-TEM images of various types of CNTs in the sample CVD-T820 $_{without\ plasma}$.

The degree of structural defects in the CNTs increases with the covalent sidewall functionalisation process. Such functionalisation can be stimulated simultaneously by the proposed synthesis method. By using the formula $d = 223.75/w$, where d (nm) is the diameter of the tubes and w (cm^{-1}) is the frequency of RBM, we can identify peaks at 211, 287 and 410 cm^{-1}. These correspond to SWCNT innermost-diameters of 1.06, 0.78, and 0.55 nm, respectively, as observed in Figs. 9(a) to (d) for *CVD-T820*$_{without\ plasma}$.

The sample *CVD-T860* is mainly composed of amorphous carbon with small traces of metal catalyst (T_{max} = 381 °C and M_{res} = 4.7) and the sample *PCVD-T860* is a mixture of MWCNT, amorphous carbon and metal catalyst (T_{max1} = 378 °C;

T_{max2} = 563 °C and M_{res} = 13.2) as shown in Figs. 10(a) and (b). The oxidation of Fe into solid oxides promoted weight gain between 185 and 320 °C for *PCVD-T860*, Fig. 8(a). The samples *CVD-T860*$_{with\ plasma}$ and *CVD-T860*$_{without\ plasma}$ have high carbon purity (over 95 wt.%), only minor contamination (metal catalyst at 5 wt.% and trace amounts of amorphous carbon), a T_{max1} in the range of 562 to 576°C, and a T_{max2} between 605-625 °C, Fig. 8(b) and Table 2. At 860°C, the T_{max2} values in the DTG plot from samples *CVD-T860*$_{with\ plasma}$ and *CVD-T860*$_{without\ plasma}$, in Fig. 10(b**)** are consistent with the formation of mixed MWCNT and SWCNTs or nanotubes with a few degrees of structural defects [29]. However, the intensities of the D-band and G-band signals are different from those of the usual SWCNTs.

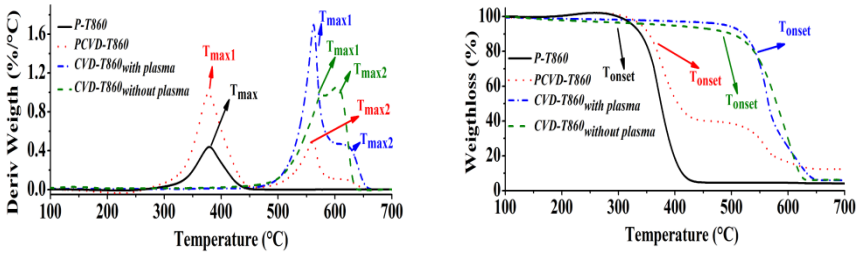

(a) TGA Plot. **(b) DTG Plot.**

Fig. 10. (a) TGA and (b) DTG profiles for carbonaceous materials extracted from the P (P-T860), PCVD (PCVD-T860) or CVD (CVD-T860 $_{with\ plasma}$) zone after synthesis by APPE-CVD at 860 °C. CVD-T860 $_{without\ plasma}$ are samples collected from the CVD chamber after reaction at 860 °C with the atmospheric pressure plasma in the off state.

It is concluded that the APP (coupled to CVD) chamber produces a mixture of CNT arrays with charge transfer effects due to chemical species attached to the CNT sidewall. Nevertheless, the CNTs (with structural defects), produced by our APPE-CVD reactor at 860 °C, exhibited higher yields and showed homogeneity among themselves. These products can be useful for various industrial and technological applications because the introduction of defects can break covalent bonds, resulting in a new chemical reactivity of the nanotube.

4. Conclusions

A reactor with horizontally aligned atmospheric-pressure plasma (APP)-enhanced CVD (APPE-CVD) has been developed to produce CNTs with high yield. The influence of operating temperature and APP on the final CNT yield has been studied. Some concluding observations from the investigation are given below:

- At 780 °C, a mixture of amorphous carbon, metal (iron) catalyst and CNTs is produced. The reaction temperature (of 780 °C) was not high enough for the synthesis of CNTs for composite applications or for their mass production.
- The optimal condition to synthesise CNTs was achieved by setting the operating temperature of the APPE-CVD reactor at 820 °C. At this

temperature, the resulting CNT arrays had a high carbon purity (95 wt. %), which is comparable with other reports.

- In contrast, at 860 °C, the formation of CNTs with different structural defects is predominant.
- By applying APP, the amount of metal catalyst in the carbonaceous deposits was reduced.
- Non-flat aluminosilicate particles were used as supports for the growth of CNTs. This increased the CNT production yields and the ease of removal of deposits from the substrate surface. The approach that we implemented may be useful to produce these nanostructures on a gram-scale for use in basic studies. The approach may also be scaled up for mass production.

Acknowledgments

This work was financially supported by DGAPA-UNAM IT100314. The authors acknowledge the technical assistance of Alejandro Tiznado, Israel Gradilla, Francisco Ruiz and Dr. Manuel Herrera-Saldivar at CNyN-UNAM. The technical assistance of Dr. Javier Camacho and Yasmin Barron at Optics Research division-CICESE (Mexico) is also gratefully acknowledged.

References

1. Iijima, S. (1991). Helical microtubules of graphitic carbon. *Nature*, 354, 56-58.
2. Liu, J.; Fan, S.; and Dai, H. (2004). Recent advances in methods of forming carbon nanotubes. *MRS Bulletin*, 29(4), 244-250.
3. Thess, A.; Lee, R.; Nikolaev, P.; Dai, H.; Petit, P.; Robert, J.; Xu, C.; Lee, Y.H.; Kim, S.G.; Rinzler, A.G.; Colbert, D.T.; Scuseria, G.E.; Tománek, D.; Fischer, J.E.; and Smalley, R.E. (1996). Crystalline ropes of metallic carbon nanotubes. *Science*, 273(5274), 483-487.
4. Journet, C.; Maser, W.K.; Bernier, P.; Loiseau, A.; de La Chapelle, M.L.; Lefrant, S.; Deniard, P.; Lee, R.; and Fischer, J.E. (1997). Large-scale production of single-walled carbon nanotubes by the electric-arc technique. *Nature*, 388), 756-758.
5. Shi, Z.; Lian, Y.; Zhou, X.; Gu, Z.; Zhang, Y.; Iijima, S.; Zhou, L.; Yue, K.T.; and Zhang, S. (1999). Mass-production of single-wall carbon nanotubes by arc discharge method. *Carbon*, 37(9), 1449-1453.
6. Hafner, J.H.; Bronikowski, M.J.; Azamian, B.R.; Nikolaev, P.; Rinzler, A.G.; Colbert, D.T.; Smith, K.A.; and Smalley, R.E. (1998). Catalytic growth of single-wall carbon nanotubes from metal particles. *Chemical Physics Letters*, 296(1-2), 195-202.
7. Kong, J.; Cassell, A.M.; and Dai, H. (1998a). Chemical vapor deposition of methane for single-walled carbon nanotubes. *Chemical Physics Letters*, 292(4-6), 567-574.
8. Shin, S.S.; Choi, B.H.; Kim, Y.M.; Lee, J.H.; and Shin, D.C. (2009). The effects of atmospheric pressure plasma on the synthesis of carbon nanotubes. *Microelectronic Engineering*, 86(4-6), 925-928.

9. Bárdos, L.; and Baránková, H. (2010). Cold atmospheric plasma: Sources, processes, and applications. *Thin Solid Films*, 518(23), 6705-6713.
10. Choi, S.I.; Nam, J.S.; Kim, J.I.; Hwang, T.H.; Seo, J.H.; and Hong, S.H. (2006). Continuous process of carbon nanotubes synthesis by decomposition of methane using an arc-jet plasma. *Thin Solid Films*, 506-507, 244-249.
11. Smiljanic, O.; Stansfield, B.L.; Dodelet, J.-P.; Serventi, A.; and Désilets, S. (2002). Gas-phase synthesis of SWNT by an atmospheric pressure plasma jet. *Chemical Physics Letters*, 356(3-4), 189-193.
12. Hahn, J.; Han, J.H.; Yoo, J.-E.; Jung, H.Y.; and Suh, J.S. (2004). New continuous gas-phase synthesis of high purity carbon nanotubes by a thermal plasma jet. *Carbon*, 42(4), 877-883.
13. Kolacyak, D.; Ihde, J.; and Lommatzsch, U.; (2011). Carbon nanotube functionalization by atmospheric pressure plasma and post-plasma reactions. *Surface and Coating Technology*, 205(Supplement 2), S605-S608.
14. Kim, D.Y.; Sugime, H.; Hasegawa, K.; Osawa, T.; and Noda, S. (2011). Sub-millimeter-long carbon nanotubes repeatedly grown on and separated from ceramic beads in a single fluidized bed reactor. *Carbon*, 49(6), 1972-1979.
15. Tiller, W.A. (1991). *The science of crystallization: microscopic interfacial phenomena*. Cambridge University Press.
16. Rinzler, A.G.; Liu, J.; Dai, H.; Nikolaev, P.; Huffman, C.B.; Rodriguez-Macias, F.J.; Boul, P.J.; Lu, A.H.; Heymann, D.; Colbert, D.T.; Lee, R.S.; Fischer, J.E.; Rao, A.M.; Eklund, P.C.; and Smalley, R.E.. (1998). Large-scale purification of single-wall carbon nanotubes: process, product, and characterization. *Applied Physics A*, 67(1), 29-37.
17. Tan, S.H.; Goak, J.C.; Hong, S.C.; and Lee, N. (2008). Purification of single-walled carbon nanotubes using a fixed bed reactor packed with zirconia beads. *Carbon*, 46(2), 245-254.
18. Mathur, R.B.; Seth, S.; Lal, C.; Rao, R.; Singh, B.P.; Dhami, T.L.; and Rao, A.M. (2007). Co-synthesis, purification and characterization of single-and multi-walled carbon nanotubes using the electric arc method. *Carbon*, 45(1), 132-140.
19. Liu, J.; and Harris, A.T. (2009). Industrially scalable process to separate catalyst substrate materials from MWNTs synthesised by fluidised-bed CVD on iron/alumina catalysts. *Chemical Engineering Science*, 64(7), 1511-1521.
20. Singh, C.; Shaffer, M.S.P.; Koziol, K.K.K.; Kinloch, I.A.; and Windle, A.H. (2003). Towards the production of large-scale aligned carbon nanotubes. *Chemical Physics Letters*, 372(5-6), 860-865.
21. Sengupta, J.; and Jacob, C. (2010). The effect of Fe and Ni catalysts on the growth of multiwalled carbon nanotubes using chemical vapor deposition. *Journal of Nanoparticle Research*, 12(2), 457-465.
22. Jak, M.J.J.; Konstapel, C.; Van Kreuningen, A.; Verhoeven, J.; and Frenken, J.W.M. (2000). Scanning tunnelling microscopy study of the growth of small palladium particles on TiO_2 (110). *Surface Science*, 457(3), 295-310.
23. Singh, C.; Shaffer, M.S.P.; and Windle, A.H.; (2003). Production of controlled architectures of aligned carbon nanotubes by an injection chemical vapor deposition method. *Carbon*, 41(2), 359-368.

24. Dichiara, A.; and Bai, J. (2012). The growth of carbon nanotube multilayers on ceramic μ-particles by catalytic chemical vapor deposition. *Diamond and Related Materials*, 29, 52-58.
25. Souza Filho, A.G.; Jorio, A.; Samsonidze, G.G.; Dresselhaus, G.; Saito, R.; and Dresselhaus, M.S. (2003). Raman spectroscopy for probing chemically/physically induced phenomena in carbon nanotubes. *Nanotechnology*, 14(10), 1130-1139.
26. Bustero, I.; Ainara, G.; Isabel, O.; Roberto, M.; Inés, R.; and Amaya, A. (2006). Control of the properties of carbon nanotubes synthesized by CVD for application in electrochemical biosensors. *Microchimica Acta*, 152(3), 239-247.
27. Saito, R.; Dresselhaus, G.; and Dresselhaus, M.S. (1998). *Physical properties of carbon nanotubes*. Imperial College.
28. Li, M.-W.; Hu, Z.; Wang, X.-Z.; Wu, Q.; Chen, Y.; and Tanian, Y.-L. (2004). Low-temperature synthesis of carbon nanotubes using corona discharge plasma at atmospheric pressure. *Diamond and Related Materials*, 13(1), 111-115.
29. Zhao, X.; Ando, Y.; Qin, L.-C.; Kataura, H.; Maniwa, Y.; and Saito, R. (2002). Radial breathing modes of multiwalled carbon nanotubes. *Chemical Physics Letters*, 361(1-2), 169-174.
30. Pedano, M.L.; and Rivas, G.A.; (2004). Adsorption and electrooxidation of nucleic acids at carbon nanotubes paste electrodes. *Electrochemistry Communications*, 6(1), 10-16.